Nat Chem. Author manuscript; available in PMC 2022 September 27.

Different timescales during ultrafast stilbene isomerisation in the gas and liquid phases revealed using time-resolved photoelectron spectroscopy

Chuncheng Wang[#1,2], **Max D.J. Waters**[#1], **Pengju Zhang**[#1,*], **Jiří Suchan**[4], **Vít Svoboda**[1], **Tran Trung Luu**[1,3], **Conaill Perry**[1], **Zhong Yin**[1], **Petr Slavíček**[4,*], **Hans Jakob Wörner**[1,*]

[1]Laboratory for Physical Chemistry, ETH Zürich, Vladimir-Prelog-Weg 2, 8093 Zürich, Switzerland

[2]Institute of Atomic and Molecular Physics, Jilin University, Changchun 130012, People's Republic of China

[3]Department of Physics, The University of Hong Kong, Pokfulam Road, SAR Hong Kong, People's Republic of China

[4]Department of Physical Chemistry, University of Chemistry and Technology Prague, Technická 5, Prague 6, 166 28, Czech Republic

[#] These authors contributed equally to this work.

Abstract

Directly contrasting ultrafast excited-state dynamics in the gas and liquid phases is crucial to understanding the influence of complex environments. Previous studies have often relied on different spectroscopic observables, rendering direct comparisons challenging. Here, we apply extreme-ultraviolet (XUV) time-resolved photoelectron spectroscopy (TRPES) to both gaseous and liquid cis-stilbene, revealing the coupled electronic and nuclear dynamics that underlie its isomerisation. Our measurements track the excited-state wave packets from excitation along the complete reaction path to the final products. We observe coherent excited-state vibrational dynamics in both phases of matter that persist to final products, enabling the characterisation of the branching space of the S_1-S_0 conical intersection. We observe a systematic lengthening of the relaxation time scales in the liquid phase and a red shift of the measured excited-state frequencies that is most pronounced for the complex reaction coordinate. These results characterise in detail the influence of the liquid environment on both electronic and structural dynamics during a complete photochemical transformation.

[*] pengju.zhang@phys.chem.ethz.ch, petr.slavicek@vscht.cz, hwoerner@ethz.ch.

Author contributions statement

HJW and CW conceived the experiments. CW, MDJW, and VS conducted the gas-phase measurements. PZ and CW conducted the liquid-phase measurements with the support of TTL, ZY, and CP. CW, PZ, TTL, VS, and MDJW performed the data analysis. JS and PS run all time-dependent calculations. MDJW provided additional *ab-initio* calculations. PZ simulated the space-charge effects. All authors contributed to the interpretation of the results and to the preparation and finalisation of the manuscript.

Competing interests statement

The authors have no competing interests to declare.

Europe PMC Funders Author Manuscripts

Abstract

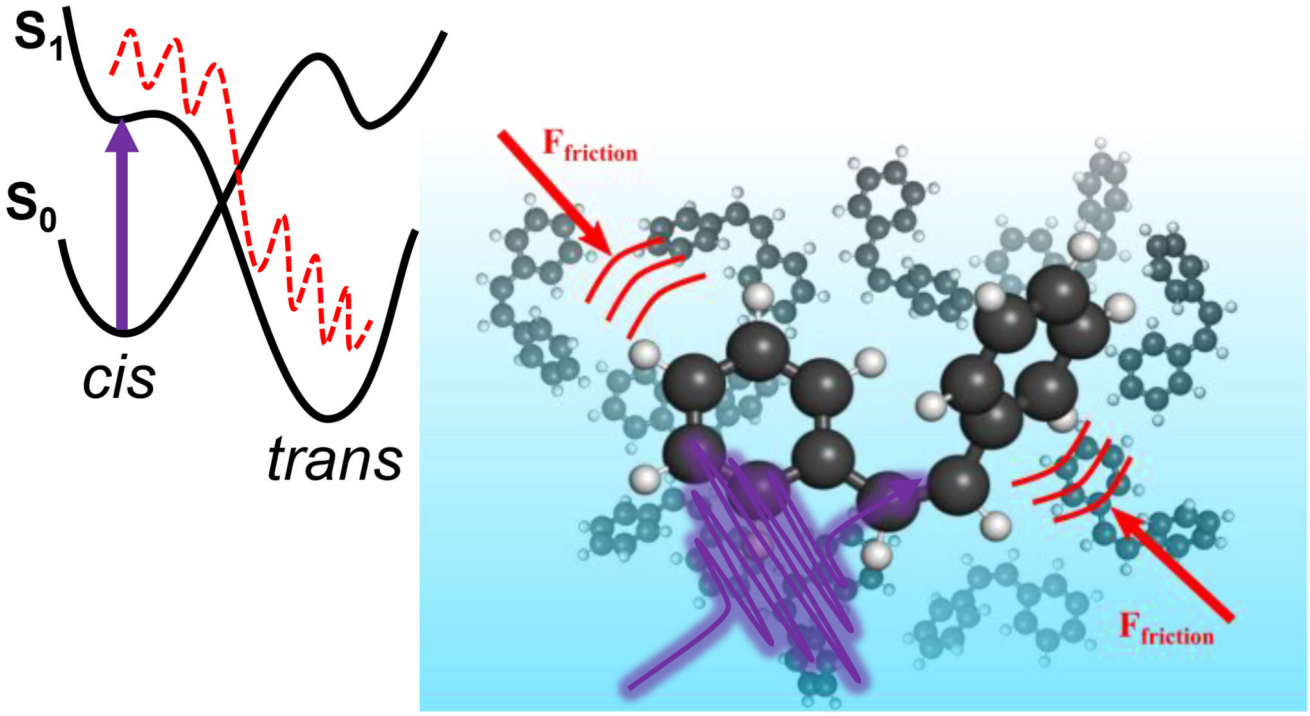

Graphic abstract.

Introduction

Most chemical reactions and biological processes occur in the liquid phase. Although it is well known that solvation can significantly modify the energetics of electronically excited states, the effects of a liquid environment on ultrafast dynamics, especially electronic and structural excited-state dynamics, are not well understood. Studies of ultrafast dynamics in the liquid phase traditionally rely on visible or ultraviolet transient-absorption spectroscopy (TAS, see e.g. Ref.[1]), which is a powerful tool, particularly in its multi-dimensional variants[2]. Despite the breadth of structural information one can obtain from TAS, one must still ultimately make assumptions about the electronic configuration of the molecule as a function of time.

Time-resolved photoelectron spectroscopy (TRPES) provides direct access to the transient electronic states and is therefore a promising alternative approach, which has mostly been exploited in the gas phase using ultraviolet probe pulses[3, 4] with recent extensions to the extreme-ultraviolet (XUV) domain[5–7]. The introduction of the liquid microjet[8] has extended the applicability of TRPES to the liquid phase, where promising results have been obtained[9–14], reaching down to the attosecond time scale[15, 16].

Previous comparisons of ultrafast dynamics in the gas and liquid phases were thus also limited to different observables, specifically TAS in the liquid phase and photo-electron/ion/

fragment spectroscopies in the gas phase (see Refs.[17, 18] and references therein). Whereas those studies yielded important insights into photodissociation and bimolecular reaction dynamics, the ultrafast structural and electronic dynamics accompanying multi-dimensional conical-intersection dynamics have eluded direct comparison across different phases of matter. Yet, such a direct comparison is arguably central for achieving a detailed understanding of the role of a complex, highly fluctuating liquid-phase environment under ambient conditions on non-adiabatic ultrafast dynamics.

In this work, we report the first comparison of ultrafast excited-state dynamics in the gas and liquid phases using the same technique, i.e. TRPES. We maximize the information content of the measurements by performing our experiments in the XUV domain, allowing us to follow the complete chemical-reaction pathway. The photoisomerisation of *cis*-stilbene is an ideal candidate for this study because it is a prototype of olefinic isomerisation dynamics[19–26] which underlie a myriad of fundamental natural processes, such as vision and germination control[27, 28].

Our study for the first time reveals vibrational coherences in both the gas- and liquid-phase data. This observation resolves an important controversy between the predictions of such vibrational coherences in Refs.[29, 30] on one hand, and their reported absence in recent gas-phase TRPES data[30] on the other. Our observations do not only clearly indicate the existence of vibrational coherences in the excited state, supported by our calculations, but even the survival of coherent wave-packet motion all the way into the electronic ground state. These observations imply that the reaction dynamics of *cis*-stilbene photoisomerisation are a more coherent process than previously assumed. Even more interestingly, this high degree of vibrational coherence is found to be robust, even in the presence of a complex, fluctuating and interacting environment. By using a high-energy probe wavelength, both the isomerisation to *trans*-stilbene and the ground-state recovery of *cis*-stilbene are observed. The associated signals reveal a long-lived vibrational coherence, originating from low-frequency phenyl-torsional modes, which provides an experimental validation of the coupling space that forms the S_1-S_0 conical intersection. Furthermore, as table-top XUV sources become more accessible, our work demonstrates both the power of using these photon ranges to collect TRPES, and a methodology for the interpretation of the complex spectra.

Our experimental results are supported by state-of-the-art electronic-structure and non-adiabatic dynamics simulations. These results show that the gas-phase TRPES can be well described when a large number of cationic states are included. Furthermore, they reveal that the friction introduced by the solvent environment is likely to be an important contribution to the condensation-induced lengthening of the relaxation time scales. Our experimental results suggest that the non-adiabatic dynamics are qualitatively similar in both phases of matter, but essentially differ in their characteristic time scales. This observation particularly applies to structural dynamics involving large-amplitude motions, which undergo the most significant lengthening upon condensation. Taken together, our methodologies offer a general protocol for unraveling the effects of a liquid environment on ultrafast coupled electronic and structural dynamics.

Results

Figure 1a illustrates our experimental approach. Using ultrashort ultraviolet (266 nm) pump and extreme-ultraviolet probe pulses, we recorded time-resolved photoelectron spectra of the *cis*-stilbene photoisomerisation in the gas and liquid phases. The specific details of the beamlines and spectrometers used in the respective experiments are given in the Methods Section. Figure 1b shows a Jabłoński diagram of the electronic states involved in the *cis-trans* isomerisation of *cis*-stilbene, and the cationic states that are accessed by the probe, in both the gas and liquid phases.

Figure 2a shows the measured spectra of *cis*-stilbene in the gas phase at pump-probe time delays between -50 fs and 1 ps (the complete TRPES spectra and global fits can be found in the supplementary information (SI) in Supplementary Fig. 1). The spectra at early delays are dominated by a broad, very short-lived photoelectron band extending from vertical binding energies (vBEs) of ~4.5-9.5 eV (black dotted box). The low-vBE region decays on a sub-picosecond time scale (red box), whereas the high-VBE region displays long-lived signals (white boxes). The high-vBE region is magnified in Fig. 2c and is further analyzed and discussed later. Based on a comparison with dynamical calculations, the signal in the black box is assigned to ionisation from the Franck-Condon (FC) region of the initially prepared S_1 state. This signal decays as a consequence of a structural relaxation from the FC region to the so-called ”phantom state” (p*), which is a low-lying, relatively flat region of the S_1 potential-energy surface, which mediates the *cis-trans* isomerisation process between the S_1 and S_0 states (see also Fig. 5).[25,29–31]. The band centred at 8.8 eV has three contributions. The contribution in the black box appears within the cross-correlation time of the experiment ((96±8) fs) and decays with a time constant of (90±30) fs. At intermediate delays (~100-400 fs), it is dominated by ionisation from S_1(p*) to a dense manifold of cationic states (D_n with n reaching up to 10). At later delays, it is dominated by ground-state recovery, including signals from *cis*- and *trans*-stilbene. The calculations supporting this assignment are shown in Supplementary Fig. 9.

The experimental data shown in Fig. 2a were analysed using a global fitting procedure, where each energy bin was fitted using a global time function. A good fit was obtained using an offset exponential function

$$S(E_k, \Delta t) = \left[\left(A_1(E_k)\mathrm{e}^{-\Delta t/\tau_1} + c\right) \times H(t)\right] \otimes G(t), \quad (1)$$

where τ_1 is the decay constant for the excited-state signal. The instrument response function is given by $G(t)$, $H(t)$ is the Heaviside step function and $A_1(E_k)$ is the amplitude of the exponential decay component for each energy bin. The obtained global fit is shown in Fig. 2b and the corresponding temporal profile, as well as τ_1 are shown in the inset of panel e. The global fit mostly captures the TRPES very well, as can be seen from the reconstructed features between 8.5 – 9.0 eV, and 6.8 – 8.0 eV. However, it is clear that the experimental transient between 5.5 – 6.5 eV decays faster than the global fit. Therefore, the photoelectron signal between 2 and 10 ps was averaged and subtracted from the spectrum with the aim of subtracting the ground-state photoelectron signal – which helps to emphasise this transient against the higher-energy photoelectron signals. This is shown in Fig. 2c, and the global fit

of this feature is shown in Fig. 2d. In this case, the best fit was obtained with a parallel biexponential decay without offset

$$S(E_k, \Delta t) = \left[\left(A_1(E_k)\mathrm{e}^{-\Delta t/\tau_1} + A_2(E_k)\mathrm{e}^{-\Delta t/\tau_2}\right) \times H(t)\right] \otimes G(t) \quad (2)$$

The obtained temporal profiles and time constants are shown in Fig. 2e. The time constant of the faster decay is consistent with that obtained from the global fit according to Eq. (1).

The results of the time-dependent non-adiabatic-dynamics simulations are shown in Fig. 2f. They included 200 trajectories, 4 neutral electronic states (S_0-S_3) and 15 cationic states (see Methods section for details). These calculations show that photoexcitation at 266 nm mainly populates the S_1 (lowest-lying bright) state, with smaller populations in the S_2 and S_3 states (Suppl. Figs. 9, 10). The observed dynamics are dominated by those of the S_1 state (Suppl. Fig. 10), on which we focus from hereon. The direct comparison of theory and experiment, reveals striking similarities which are highlighted by the dashed boxes, facilitating a direct comparison of Fig. 2a and f. Both show a strong signal from higher-lying cationic states at short time delays around 8.8 eV, with the excited-state signal decaying within ~400 fs. The signal observed at longer delays, corresponding to ionization of the photoexcited wave packet that has returned to the electronic ground state, also agrees very well. The regions highlighted by the red rectangle also agree well, although the decay of the S_1(p*) signal is faster in the calculation than in the experiment. The time scale of the calculated decay is in good agreement with the most recent *ab-initio* multiple spawning calculations[29, 30]. The shorter calculated decay time scale might be the consequence of zero-point leakage, i.e. a higher effective temperature in the calculations. The experimentally observed decay in the region of 7-8 eV is also well reproduced by the calculations, although the calculations underestimate (overestimate) the signal around binding energies of 6.2 eV (7.8 eV). The calculations predict a strong, rapidly decaying signal below 5 eV, which is less clear in the experimental data, possibly due to the finite experimental cross-correlation time, as opposed to the impulsive excitation assumed in the calculations. Finally, we note that the experimental signal at all binding energies appears more slowly for the same reason.

The experimental TRPES of liquid-phase *cis*-stilbene is shown in Fig. 3a with the global fit of this data being shown in panel b. The time function that gave the best fit differs slightly from the gas-phase results, in that it is a sequential (rather than a simultaneous) biexponential model. The sequential biexponential decay is described as

$$S(E_k, \Delta t) = \left[\left(A_1(E_k)\mathrm{e}^{-\Delta t/\tau_1} + A_2(E_k)\left(1 - \mathrm{e}^{-\Delta t/\tau_1}\right)\mathrm{e}^{-\Delta t/\tau_2}\right) \times H(t)\right] \otimes G(t) \quad (3)$$

where the decay constant τ_1 is the same as the rise time of the second exponential decay. The one-dimensional decay profile of this model is shown in Fig. 3d, and the calculated TRPES from the dynamical simulations is shown in panel c.

In the experimental TRPES in Fig. 3a, we first note the overall shift of the signal to lower binding energies by ~1 eV, a consequence of solvent polarization. At early delays up to ~200 fs, we particularly note the rapid decay of the band between 3.1 eV, and 3.9 eV, which is

assigned to relaxation out of the Franck-Condon region by comparison with the calculations shown in Fig. 3c. At longer time delays, the spectrum is dominated by a broad band centered at 4.7 eV, which is reminiscent of the excited-state gas-phase signal, shown in Fig. 2c, and also corresponds to the decay of the S_1(p*) signal. The primary temporal difference between the corresponding photoelectron signals is the longevity of the liquid-phase transient. The gas-phase excited-state signal has been fitted with a monoexponential decay, yielding a decay constant of (426±28) fs, whereas the liquid-phase signal remains in the excited state for much longer, with a decay constant of (1029±157) fs. This is also reflected by the theoretical simulations shown in Fig. 3c, where the excited-state signal is still reasonably strong after a picosecond, in contrast to the corresponding gas-phase calculation (Fig. 2f).

Following excitation at 266 nm the S_1 state is mainly populated (Supplementary Fig. 10). Our measurements (Fig. 3a) show a very short-lived transient at vBEs between 3.3-4.0 eV, which we assign to relaxation out of the Franck-Condon region. The p* region of the S_1 state dominates the measured excited-state transient at longer time delays, both in the gas and liquid phases (Fig. 2c for the gas phase, and the photoelectron signal between ~6.5 and 4.0 eV in Fig. 3a).

In the liquid phase, the rise time of the p* signal (blue curve in Fig. 3d) is thus explicitly correlated to the decay time of the signal from the Franck-Condon region, with a time constant of (208±97) fs. In the gas phase, the decay of the signal from the Franck-Condon region and the rise time of the p* signal are both within the cross-correlation time. The transient p* signals are the dominant and longest-lived features for both liquid and gas phases. Interestingly, the liquid-phase p* signal appears more slowly with a rise time of (208±97) fs. The decay time of the liquid-phase signal p* is about two times longer than in the gas phase.

One of the main advantages of using an XUV probe is its ability to follow the excited-state dynamics all the way to the electronic ground state. As will become evident from the Fourier analysis shown below, coherent vibrational dynamics are observed in the gas-phase photoelectron signals of both the ground (Fig. 2a) and electronically excited (Fig. 2c) states. The intensity of the ground-state photoelectron signal displays a long-lived oscillation (Fig. ??). A Fourier transform of this signal (Fig. 4a) gives a number of distinct frequencies that can all be assigned to the overtones of the phenyl torsional mode of the electronic ground state of *trans*-stilbene. The measured frequencies from the literature are shown in parentheses for comparison[32]. This observation suggests that the phenyl torsion is one of the two vibrational modes spanning the branching space of the CI that mediates the *cis-trans* isomerisation. This conclusion is indeed confirmed by our *ab-initio* calculations (SI, Section 7). Moreover, coherent oscillations are also present in the p* signal (Fig. 2c,e). The Fourier transform of the corresponding residuals is shown in Fig. 4b. These frequencies can mostly be assigned to excited-state phenyl torsional motions[32] of the *cis*-stilbene S_1 state (p* region), except for 365 cm^{-1}, which is assigned to the ethylenic torsion of the complex reaction coordinate[25, 33].

Turning to the liquid phase, oscillations in the p* signal are also visible (Fig. 3d), and their Fourier spectrum is presented in Fig. 4c. Just as in the gas phase, the peak at 175

cm^{-1} is assigned to excited-state phenyl torsion motion. The higher frequency of 323 cm^{-1} in the liquid phase matches with the ethylenic torsion of the complex reaction coordinate. This red shift of this frequency compared to the gas phase amounts to 42 cm^{-1}, which is mainly assigned to frictional forces in the liquid phase that hinder the corresponding large-amplitude motion.

Discussion

Our experimental results combined with theoretical calculations lead to the following comprehensive picture of the isomerisation dynamics. The excited-state dynamics of *cis*-stilbene are characterised by two concerted nuclear motions, as graphically outlined in Fig. 5. The first is pyramidalisation of the ethylenic carbons, very similar to hydrogen-out-of-plane (HOOP) motions[29, 34, 35]. The second motion is a dihedral rotation around the central ethylenic bond. The Fourier transform of the experimental TRPES of the p* region reveals frequencies (Fig. 4b) that correspond to the ethylenic dihedral motion of *cis*-stilbene.[25] This motion is part of a complex reaction coordinate that leads to the S_1-S_0 conical intersection. The fact that these vibrational coherences appear is a strong indication of coherent non-adiabatic dynamics in the electronically excited state of *cis*-stilbene. The preservation of coherence is further reflected in the Fourier transform of the ground-state photoelectron signal between 2 and 10 ps, around 9 eV in the experimentally measured TRPES in Fig. ?? a. This Fourier transform is shown in Fig. 4a, and corresponds to low-frequency phenyl torsional modes, which are a vibrational fingerprint of the coupling space of the S_1-S_0 conical intersection, as further consolidated by calculations shown in the SI (section 7). This interpretation is consistent with previous computational modelling which showed how kinetic energy from motion along the direction of the coupling vectors is redistributed into the phenyl torsional motions[26, 29, 36].

The liquid-phase TRPES displayed excited-state dynamics that is similar to the gas phase, though with important differences. In the gas phase, a parallel biexponential decay gives the best agreement with the measured data, whereas the liquid-phase data requires a sequential biexponential decay. It should be stressed that this is not necessarily an indication of different dynamics, but is most likely the consequence of a systematic lengthening of the relaxation time scales. The first decay would thus correspond to relaxation out of the Franck-Condon region towards the p* region, which in the gas phase happens on a time scale very similar to the cross-correlation time, as it corresponds to HOOP motions. This is supported by previous studies who found that this relaxation takes place in <25 fs in the gas phase.[29, 34, 35]

The effect of the liquid environment on the *cis*-stilbene photodynamics has been qualitatively modeled with the Langevin equation, introducing friction and random forces. It is well known e.g. from the studies on trans-stilbene photodynamics that frequency-dependent friction terms would be needed to model such effects quantitatively[37]. However, even the simple approach with a constant friction term predicts a noticeable lengthening of the relaxation time scales, in agreement with our observations.

Despite these differences, there is a key similarity between the liquid-phase data and the gas-phase data in terms of the observed vibrational coherences. This is manifested in the close agreement between the two Fourier spectra of the p* signals (Figs. 4b,c). The highest-frequency peak 365/323 cm^{-1}, is assigned to the ethylenic torsion, which forms the primary motion of the *cis-trans* isomerisation coordinate. This motion is characteristic of the excited-state wave packet oscillating in a local minimum of the p* region. Comparison of the frequencies reveals a red shift in the liquid phase, which is largest (42 cm^{-1}) for the ethylenic torsion. This can be rationalised by the friction imposed by the liquid environment, which is most significant for the largest-amplitude motion, as illustrated in Fig. 3f.

Although coherent vibrational motion in the liquid phase has been previously observed[38–42], it might seem remarkable that such a large-amplitude motion as torsion of the ethylenic dihedral angle would be able to maintain coherence. Indeed, steric interactions with the solvent could be expected to be sufficient for the molecule to start favouring dissipation of its internal energy into the various bath modes available. In the case of isolated molecules, the vibrational coherence is preserved due to the relaxation pathways to both the p* region and the ground state featuring no potential-energy barrier. The observed preservation of coherence suggests that the effects of the liquid-phase environment are not sufficient to modify or create a barrier on the gas-phase relaxation pathway. This could possibly explain why the ethylenic chromophore has been so evolutionary favourable in liquid-phase biological processes that require a chemical switch - for example, the photoisomerisation of rhodopsin.

Before concluding, it is worth pointing out that our results contain no indications of the formation of 4a,4b-dihydrophenanthrene (DHP). The TRPES spectra show no clear evidence for its formation and none of the calculated trajectories predict its appearance. It is therefore likely to be a minor channel under the conditions of the present experiments. It is also worth noting that our liquid-phase measurements have been done on neat stilbene to avoid dilution-induced signal reduction. In the future, it will be interesting to study the influence of other solvent environments on the reported isomerisation dynamics and coherences.

Conclusions

In summary, XUV probe photons have enabled us to follow the complete reaction paths of the photoisomerisation of *cis*-stilbene in both the gas and liquid phases and to directly compare them using the same observables. Qualitative similarities in the relaxation pathways, combined with quantitative differences in the time scales have been observed. Relaxation out of the Franck-Condon region was found to occur on time scales of (118±18) fs and (208±97) fs in the gas and liquid phases, respectively, whereas non-adiabatic relaxation from the p* region to the electronic ground state were found to occur in (426±28) fs and (1029±157) fs. These dynamics were assigned through comparison with non-adiabatic-dynamics calculations. The lengthening of the time scales by a factor of ~2 in the liquid phase was at least partially assigned to the effect of friction on the large-amplitude molecular motion. Importantly, long-lived vibrational coherences in the electronic ground state of stilbene, surviving internal conversion in both phases of matter have also been observed, thereby revealing that the *cis-trans* isomerisation is a remarkably coherent process.

Europe PMC Funders Author Manuscripts

This work demonstrates the considerable potential of XUV-TRPES in building bridges that connect liquid-phase chemical-reaction dynamics with those of isolated gas-phase molecules, opening a new pathway to a detailed understanding of the coupled electronic and nuclear dynamics contributing to chemical-reaction dynamics in the liquid phase.

Methods

Two complementary experimental setups were employed in this study. For the liquid-phase measurements, XUV probe pulses obtained from high-harmonic generation (HHG) were combined with pump pulses centered at 266 nm in the interaction region of a magnetic-bottle photoelectron spectrometer, as shown in Extended Data Figure 1. The XUV pulses were provided by a time-preserving monochromator[43]. The 1.6 mJ pulses with a duration of 30-fs centered at 800 nm at a repetition rate of 5-kHz were split into two arms using an 80:20 beamsplitter. The major reflected beam was focused into a semi-infinite gas cell filled with 10 mbar Xe to drive HHG. The generated high-order harmonics were first spatially selected by a 300 lines/mm grating and then focused with a toroidal mirror into the interaction region (focal diameter: ~250 μm). The minor transmitted beam was used to produce 266 nm pump pulses by mixing the fundamental 800 nm with the second harmonic at 400 nm in a type I process in BBO, and the 266-nm beam was focussed into the chamber with a focal diameter of ~150 μm. The delay between the two pulses was set by changing the optical path length of the 266 nm pulses using a motorised translation stage. Photoelectron spectra of rare gases were used for energy calibration of the photoelectron spectrometer. The needle valve for the gas-phase experiment and the 35 μm quartz nozzle generating the microjet for the liquid-phase experiment were both mounted on a grounded PEEK holder. The quartz nozzle was capped with Cu tape, held together by Sn solder, to prevent the insulating quartz from charging up due to stray electrons[44]. The liquid *cis*-stilbene was purchased from abcr swiss AG and was recycled for multiple measurement purpose, its purity was repeatedly analysed by a commercial gas chromatograph from ThermoFisher Scientific (Model:TRACE 1300) after each recycle. Our liquid sample contains 99.2% of *cis*-stilbene and 0.8% of *trans*-stilbene. The small amount of *trans*-stilbene will not affect our results, owing to the long-lived character (~100 ps) of its S_1 state. Tetrabutylammonium chloride is dissolved in *cis*-stilbene to a concentration of 50 mmol/l to minimize electrokinetic charging. The experiments were run with a liquid flow rate of 0.4 mL/min.

For the gas-phase measurements, 266-nm pump and 133-nm probe pulses are combined in a home-built velocity-map imaging (VMI) spectrometer[45, 46]. The parameters of the laser pulses and beam paths are indicated in Extended Data Figure 2. 3 mJ pulses with a duration of 30 fs centered at 800 nm are split into two arms using an 80:20 beam splitter. The major component of the beam is frequency-doubled in a BBO and then used to generate low-order harmonics of 400 nm in a semi-infinite gas cell filled with 10 mbar of Xe, resulting in 133 nm laser light[47]. The minor component is used to generate 266 nm pulses which are used as the pump in this experiment. The cis−stilbene is delivered into the chamber by flowing 2 bar He through a bubbler containing the liquid sample. The photoelectrons created by ionisation of the gaseous sample are accelerated by the extractor and repeller plates and then detected

through an imaging system consisting of a microchannel-plate detector, a phosphor screen and a CCD camera.

The non-adiabatic simulations of cis-stilbene upon the photoexcitation into the first absorption band were performed with the Landau-Zener surface hopping (LZSH) algorithm.[48, 49] LZSH is a multi-dimensional and adiabatic version of the Landau-Zener surface hopping method where the transition probabilities are evaluated based on the curvature of the potential energy surface along the trajectory. The main advantage of the LZSH scheme is that it does not require knowledge of non-adiabatic coupling elements for the evaluation of the transition probabilities. We have calculated 200 trajectories for both the gas phase and the liquid phase for 1.2 ps, with a time step of 0.12 fs. In our simulations, 4 electronic states were included; with this choice, the bright, absorbing state was always covered. The initial conditions for the LZSH simulations were evaluated within molecular dynamics simulations with a quantum thermostat based on the Generalised Langevin equation (GLE).[50] The GLE quantum thermostat approach covers the zero-point energy delocalisation exactly for harmonic modes and the initial state is captured reasonably even for modes with medium anharmonicity.[51] For the liquid phase, we modeled the effect of the environment by coupling all atoms of the system to the Langevin thermostat with a time constant τ =1.0 ps and τ =0.5 ps. We have assumed a temperature of 300 K in all the simulations. The molecular dynamics (MD) calculations were run within our in-house code ABIN.[52] The parameters for the GLE thermostat were taken from an online database.[53]

The MD calculations used energies and forces calculated within the multi-reference configuration interaction method built upon a semi-empirical orthogonalisation (OM3) parametrisation based on the MNDO-type Hamiltonian.[54] This approach was shown to work well for various systems,[55] noticeably the combination provided faithful results for cis-trans isomerisation processes in combination with the LZSH scheme.[56] We considered 6 occupied and 11 unoccupied orbitals in our active space. For correlation treatment, graphical unitary group approach (GUGA-CI). MR-CISD/OM3 were performed in the MNDO2005 7.0 program.[57]

The time-dependent signal corresponding to the time-resolved photoelectron spectra was modeled by calculating the density of electronic states along the trajectory; we also considered varying contributions of the distinct electronic states to the signal, i.e. the Dyson norms were evaluated. The ionisation energies were calculated with the CASSCF(16/10)/6-31g* approach, considering 8 occupied and 2 unoccupied orbitals in the active space, state-averaging over 4 neutral excited and 15 ionized states. The ionization energies were then shifted to match the first ionization energy of the MR-CISD/OM3 approach. We have further tested the energetics against the CASPT2 calculations, see the Supplementary Information. The CASSCF and CASPT2 calculations were performed in the MOLPRO 2012 package.[58] The Dyson norms were evaluated using WFOVERLAP program within SHARC suite.[59] For the liquid phase calculations, we have added a constant solvent shift of 1.05 eV for all ionic states. The value was calculated within a polarisable continuum model using the concept of non-equilibrium solvation (see the Supporting Information for more details). Finally, we have subtracted the signal calculated at $t = 0$ from the signal calculated at a given time. The quantity calculated in this way is directly comparable to the experiment.

Europe PMC Funders Author Manuscripts

Extended Data

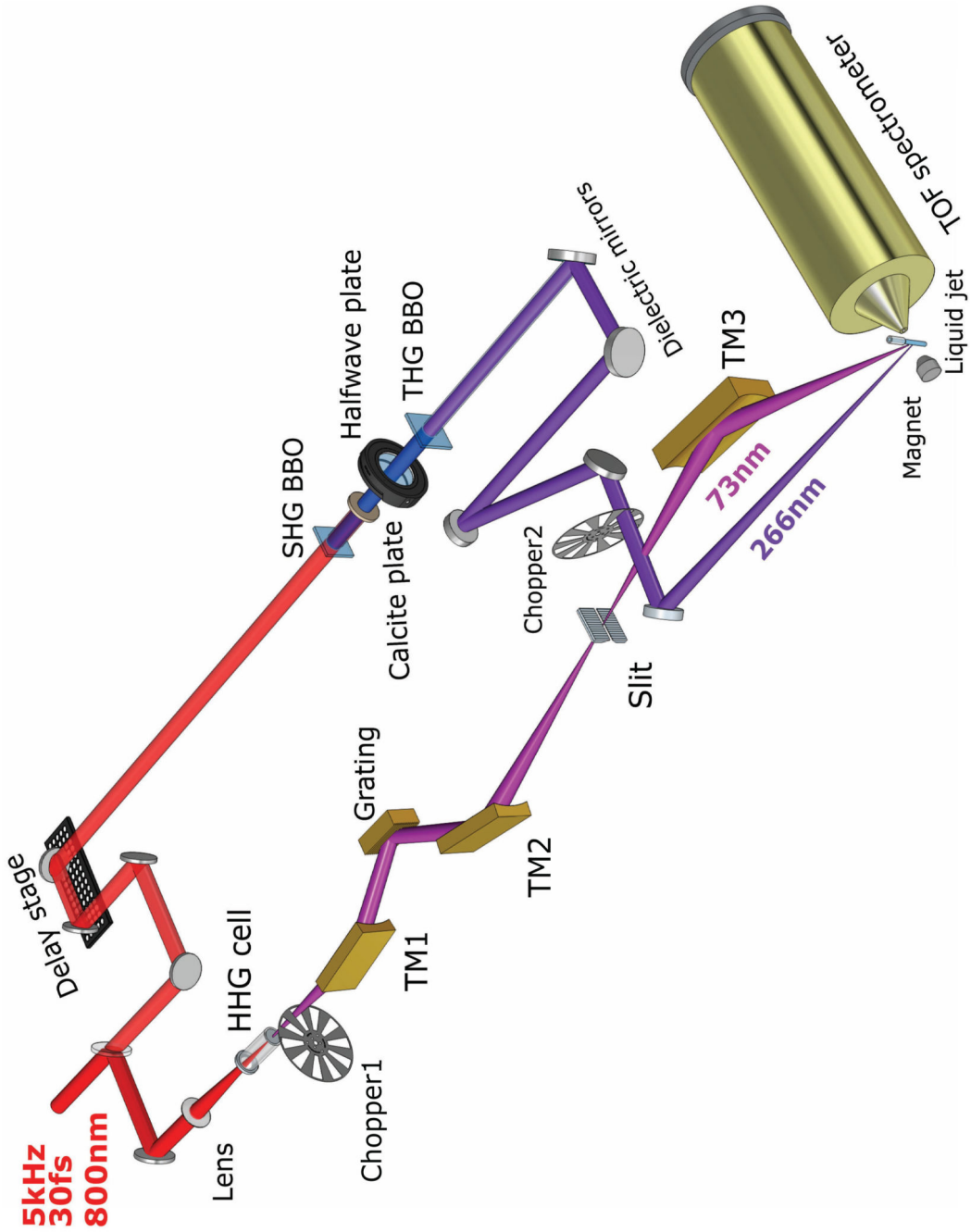

Extended Data Figure 1. The experimental setup for the liquid-phase TRPES measurements.

Europe PMC Funders Author Manuscripts

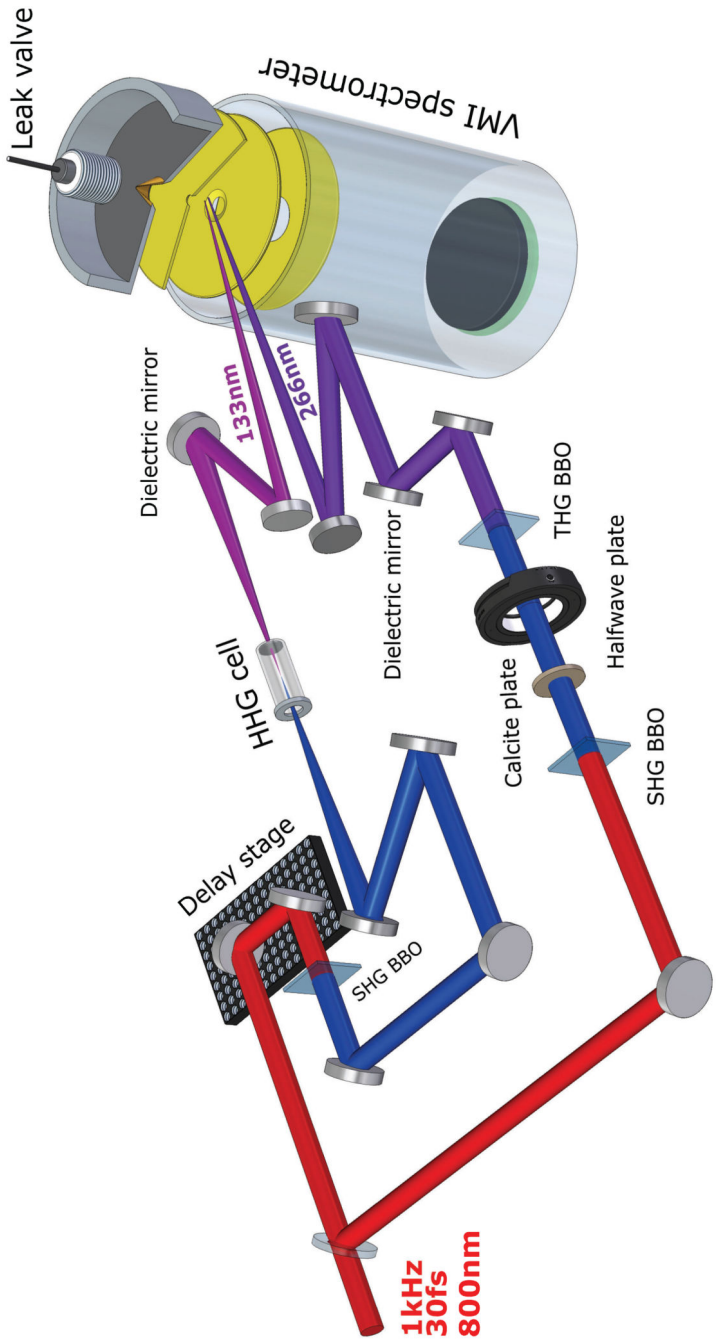

Extended Data Figure 2. The experimental setup for the gas-phase measurements.

Supplementary Material

Refer to Web version on PubMed Central for supplementary material.

Acknowledgements

We thank Todd Martinez, Hayley Weir and Monika Williams for discussions and for providing the data shown in Suppl. Fig. 7a. We acknowledge financial support from ETH Zürich and the Swiss National Science Foundation

through grant 200021_172946 (HJW). ZY acknowledges financial support from an ETH Career Seed Grant No SEED-12 19-1. CW additionally acknowledges support from the National Natural Science Foundation of China (Grant No.11534004, 11627807, 11774130) and the financial support from Jilin University.

Data Availability

The data generated or analysed during this study are included in this published article (and its supplementary information file).

References

1. Polli D, et al. Conical intersection dynamics of the primary photoisomerization event in vision. Nature. 2010; 467: 440–443. DOI: 10.1038/nature09346 [PubMed: 20864998]
2. Engel GS, et al. Evidence for wavelike energy transfer through quantum coherence in photosynthetic systems. Nature. 2007; 446: 782–786. DOI: 10.1038/nature05678 [PubMed: 17429397]
3. Cyr DR, Hayden CC. Femtosecond time-resolved photoionization and photoelectron spectroscopy studies of ultrafast internal conversion in 1, 3, 5-hexatriene. J chemical physics. 1996; 104: 771–774. DOI: 10.1063/1.470802
4. Neumark DM. Time-resolved photoelectron spectroscopy of molecules and clusters. Annu Rev Phys Chem. 2001; 52: 255. doi: 10.1146/annurev.physchem.52.1.255 [PubMed: 11326066]
5. von Conta A, et al. Conical-intersection dynamics and ground-state chemistry probed by extreme-ultraviolet time-resolved photoelectron spectroscopy. Nat Commun. 2018; 9 3162 doi: 10.1038/s41467-018-05292-4 [PubMed: 30089780]
6. Smith AD, et al. Mapping the complete reaction path of a complex photochemical reaction. Phys Rev letters. 2018; 120 183003 doi: 10.1103/PhysRevLett.120.183003
7. Squibb RJ, et al. Acetylacetone photodynamics at a seeded free-electron laser. Nat Commun. 2018; 9: 63. doi: 10.1038/s41467-017-02478-0 [PubMed: 29302026]
8. Faubel M, Steiner B, Toennies JP. Photoelectron spectroscopy of liquid water, some alcohols, and pure nonane in free micro jets. The J chemical physics. 1997; 106: 9013–9031. DOI: 10.1063/1.474034
9. Suzuki Y-I, et al. Isotope effect on ultrafast charge-transfer-to-solvent reaction from i-to water in aqueous nai solution. Chem Sci. 2011; 2: 1094–1102. DOI: 10.1039/C0SC00650E
10. Elkins MH, Williams HL, Shreve AT, Neumark DM. Relaxation mechanism of the hydrated electron. Science. 2013; 342: 1496–1499. DOI: 10.1126/science.1246291 [PubMed: 24357314]
11. Thürmer S, et al. Photoelectron angular distributions from liquid water: Effects of electron scattering. Phys Rev Lett. 2013; 111 173005 doi: 10.1103/PhysRevLett.111.173005 [PubMed: 24206487]
12. Ojeda J, Arrell CA, Longetti L, Chergui M, Helbing J. Charge-transfer and impulsive electronic-to-vibrational energy conversion in ferricyanide: ultrafast photoelectron and transient infrared studies. Phys Chem Chem Phys. 2017; 71 17052 doi: 10.1039/C7CP03337K
13. Riley JW, et al. Unravelling the role of an aqueous environment on the electronic structure and ionization of phenol using photoelectron spectroscopy. The journal physical chemistry letters. 2018; 9: 678–682. DOI: 10.1021/acs.jpclett.7b03310
14. Nishitani J, Yamamoto Y-i, West CW, Karashima S, Suzuki T. Binding energy of solvated electrons and retrieval of true uv photoelectron spectra of liquids. Sci advances. 2019; 5 eaaw6896 doi: 10.1126/sciadv.aaw6896 [PubMed: 31497644]
15. Jordan I, Huppert M, Brown MA, van Bokhoven JA, Wörner HJ. Photoelectron spectrometer for attosecond spectroscopy of liquids and gases. Rev Sci Instruments. 2015; 86 123905 doi: 10.1063/1.4938175
16. Jordan I, et al. Attosecond spectroscopy of liquid water. Science. 2020; 369: 974–979. DOI: 10.1126/science.abb0979 [PubMed: 32820124]
17. Crim FF. Molecular reaction dynamics across the phases: similarities and differences. Faraday discussions. 2012; 157: 9–26. DOI: 10.1039/C2FD20123B [PubMed: 23230761]

18. Harris SJ, et al. Comparing molecular photofragmentation dynamics in the gas and liquid phases. Phys Chem Chem Phys. 2013; 15: 6567–6582. DOI: 10.1039/c3cp50756d [PubMed: 23552482]
19. Syage J, Lambert WR, Felker P, Zewail A, Hochstrasser R. Picosecond excitation and trans-cis isomerization of stilbene in a supersonic jet: Dynamics and spectra. Chem Phys Lett. 1982; 88: 266–270. DOI: 10.1016/0009-2614(82)87085-1
20. Troe J, Weitzel K-M. Mndo calculations of stilbene potential energy properties relevant for the photoisomerization dynamics. The J chemical physics. 1988; 88: 7030–7039. DOI: 10.1063/1.454402
21. Sension R, Repinec S, Hochstrasser R. Femtosecond laser study of energy disposal in the solution phase isomerization of stilbene. J chemical physics. 1990; 93: 9185–9188. DOI: 10.1063/1.459707
22. Waldeck DH. Photoisomerization dynamics of stilbenes in polar solvents. J Mol Liq. 1993; 57: 127–148. DOI: 10.1016/0167-7322(93)80051-V
23. Nikowa L, Schwarzer D, Troe J, Schroeder J. Viscosity and solvent dependence of low-barrier processes: Photoisomerization of cis-stilbene in compressed liquid solvents. The J chemical physics. 1992; 97: 4827–4835. DOI: 10.1063/1.463837
24. Rodier JM, Myers AB. cis-stilbene photochemistry: solvent dependence of the initial dynamics and quantum yields. J Am Chem Soc. 1993; 115: 10791–10795. DOI: 10.1021/ja00076a041
25. Takeuchi S, et al. Spectroscopic tracking of structural evolution in ultrafast stilbene photoisomerization. Science. 2008; 322: 1073–1077. DOI: 10.1126/science.1160902 [PubMed: 19008439]
26. Quenneville J, Martínez TJ. Ab initio study of cis-trans photoisomerization in stilbene and ethylene. J Phys Chem A. 2003; 107: 829–837. DOI: 10.1021/jp021210w
27. Schoenlein R, Peteanu L, Mathies R, Shank C. The first step in vision: femtosecond isomerization of rhodopsin. Science. 1991; 254: 412–415. DOI: 10.1126/science.1925597 [PubMed: 1925597]
28. Willner I, Rubin S. Control of the structure and functions of biomaterials by light. Angewandte Chemie Int Ed Engl. 1996; 35: 367–385. DOI: 10.1002/anie.199603671
29. Weir H, Williams M, Parrish RM, Hohenstein EG, Martínez TJ. Nonadiabatic dynamics of photoexcited cis-stilbene using ab initio multiple spawning. J Phys Chem B. 2020; 124: 5476–5487. DOI: 10.1021/acs.jpcb.0c03344 [PubMed: 32428407]
30. Williams M, et al. Unmasking the cis-stilbene phantom state via vacuum ultraviolet time-resolved photoelectron spectroscopy and ab initio multiple spawning. The J Phys Chem Lett. 2021; 12: 6363–6369. DOI: 10.1126/science.1925597 [PubMed: 34231356]
31. Fuß W, Kosmidis C, Schmid W, Trushin S. The lifetime of the perpendicular minimum of cis-stilbene observed by dissociative intense-laser field ionization. Chem Phys Lett. 2004; 385: 423–430. DOI: 10.1016/j.cplett.2003.12.114
32. Chiang W-Y, Laane J. Fluorescence spectra and torsional potential functions for trans-stilbene in its S_0 and S_1 (π, π^*) electronic states. J Chem Phys. 1994; 100: 8755–8767. DOI: 10.1063/1.466730
33. Kwok WM, et al. Time-resolved resonance raman study of s1 cis-stilbene and its deuterated isotopomers. J Raman Spectrosc. 2003; 34: 886–891. DOI: 10.1002/jrs.1070
34. Kukura P. Structural observation of the primary isomerization in vision with femtosecond-stimulated raman. Science. 2005; 310: 1006–1009. DOI: 10.1126/science.1118379 [PubMed: 16284176]
35. Schapiro I, et al. The ultrafast photoisomerizations of rhodopsin and bathorhodopsin are modulated by bond length alternation and HOOP driven electronic effects. J Am Chem Soc. 2011; 133: 3354–3364. DOI: 10.1021/ja1056196 [PubMed: 21341699]
36. Fdez Galván I, Delcey MG, Pedersen TB, Aquilante F, Lindh R. Analytical state-average complete-activespace self-consistent field nonadiabatic coupling vectors: Implementation with density-fitted two-electron integrals and application to conical intersections. J Chem Theory Comput. 2016; 12: 3636–3653. DOI: 10.1021/acs.jctc.6b00384 [PubMed: 27327873]
37. Pollak E. Transition state theory for photoisomerization rates of trans-stilbene in the gas and liquid phases. The J Chem Phys. 1987; 86: 3944–3949. DOI: 10.1063/1.451903
38. Chudoba C, Riedle E, Pfeiffer M, Elsaesser T. Vibrational coherence in ultrafast excited state proton transfer. Chem Phys Lett. 1996; 263: 622–628. DOI: 10.1016/s0009-2614(96)01268-7

2. Takeuchi S, Tahara T. Femtosecond absorption study of photodissociation of diphenylcyclopropenone in solution: reaction dynamics and coherent nuclear motion. J Chem Phys. 2004; 120: 4768–4776. DOI: 10.1063/1.1645778 [PubMed: 15267337]

40. Takeuchi S, Tahara T. Coherent nuclear wavepacket motions in ultrafast excited-state intramolecular proton transfer: sub-30-fs resolved pump-probe absorption spectroscopy of 10-hydroxybenzo[h]quinoline in solution. J Phys Chem A. 2005; 109: 10199–10207. DOI: 10.1021/jp0519013 [PubMed: 16833312]

41. Monni R, et al. Vibrational coherence transfer in the ultrafast intersystem crossing of a diplatinum complex in solution. Proc Natl Acad Sci. 2018; 115: E6396–E6403. DOI: 10.1073/pnas.1719899115 [PubMed: 29941568]

42. Banin U, Waldman A, Ruhman S. Ultrafast photodissociation of I3-in solution: Direct observation of coherent product vibrations. J Chem Phys. 1992; 96: 2416–2419. DOI: 10.1063/1.462041

43. von Conta A, Huppert M, Wörner HJ. A table-top monochromator for tunable femtosecond xuv pulses generated in a semi-infinite gas cell: Experiment and simulations. Rev Sci Instruments. 2016; 87 doi: 10.1063/1.4955263

44. Perry CF, et al. Ionization energy of liquid water revisited. J Phys Chem Lett. 2020; 11: 1789–1794. DOI: 10.1021/acs.jpclett.9b03391 [PubMed: 31977222]

45. Walt SG, et al. Role of multi-electron effects in the asymmetry of strong-field ionization and fragmentation of polar molecules: The methyl halide series. J Phys Chem A. 2015; 119: 11772–11782. DOI: 10.1021/acs.jpca.5b07331 [PubMed: 26565126]

46. Walt SG, et al. Dynamics of valence-shell electrons and nuclei probed by strong-field holography and rescattering. Nat Comm. 2017; 8 15651 doi: 10.1038/ncomms15651

47. Svoboda V, Ram NB, Rajeev R, Wörner HJ. Time-resolved photoelectron imaging with a femtosecond vacuumultraviolet light source: Dynamics in the Ã/B̃-and F̃-bands of SO_2. J Chem Phys. 2017; 146 084301 doi: 10.1063/1.4976552 [PubMed: 28249458]

48. Belyaev AK, Lasser C, Trigila G. Landau–Zener type surface hopping algorithms. The J Chem Phys. 2014; 140 224108 doi: 10.1063/1.4882073 [PubMed: 24929375]

49. Suchan J, Janoš J, Slavíček P. Pragmatic Approach to Photodynamics: Mixed Landau–Zener Surface Hopping with Intersystem Crossing. J Chem Theory Comput. 2020; 16: 5809–5820. DOI: 10.1021/acs.jctc.0c00512 [PubMed: 32687703]

50. Ceriotti M, Bussi G, Parrinello M. Colored-noise thermostats àla Carte. J Chem Theory Comput. 2010; 6: 1170–1180. DOI: 10.1021/ct900563s arXiv:1204.0822v1

51. Hollas D, Muchová E, Slavíček P. Modeling Liquid Photoemission Spectra: Path-Integral Molecular Dynamics Combined with Tuned Range-Separated Hybrid Functionals. J Chem Theory Comput. 2016; 12: 5009–5017. DOI: 10.1021/acs.jctc.6b00630 [PubMed: 27654577]

52. Hollas, D; Suchan, J; Ončák, M; Slavícek, P. PHOTOX/ABIN v11. 2018.

53. GLE4MD input library.

54. Dral PO, et al. Semiempirical Quantum-Chemical Orthogonalization-Corrected Methods: Theory, Implementation, and Parameters. J Chem Theory Comput. 2016; 12: 1082–1096. DOI: 10.1021/acs.jctc.5b01046 [PubMed: 26771204]

55. Silva-Junior MR, Thiel W. Benchmark of Electronically Excited States for Semiempirical Methods: MNDO, AM1, PM3, OM1, OM2, OM3, INDO/S, and INDO/S2. J Chem Theory Comput. 2010; 6: 1546–1564. DOI: 10.1021/ct100030j [PubMed: 26615690]

56. Janoš J, et al. Conformational control of the photodynamics of a bilirubin dipyrrinone subunit: Femtosecond spectroscopy combined with nonadiabatic simulations. The J Phys Chem A. 2020; 124: 10457–10471. DOI: 10.1021/acs.jpca.0c08945 [PubMed: 33283519]

57. Dewar MJ, Thiel W. Ground states of molecules. 38. the mndo method. approximations and parameters. J Am Chem Soc. 1977; 99: 4899–4907. DOI: 10.1002/chin.197744060

58. Werner H-J, Knowles PJ, Knizia G, Manby FR, Schütz M. Molpro: a general-purpose quantum chemistry program package. Wiley Interdiscip Rev Comput Mol Sci. 2012; 2: 242–253. DOI: 10.1002/wcms.82

59. Plasser F, et al. Efficient and flexible computation of many-electron wave function overlaps. J Chem Theory Comput. 2016; 12: 1207–1219. DOI: 10.1021/acs.jctc.5b01148 [PubMed: 26854874]

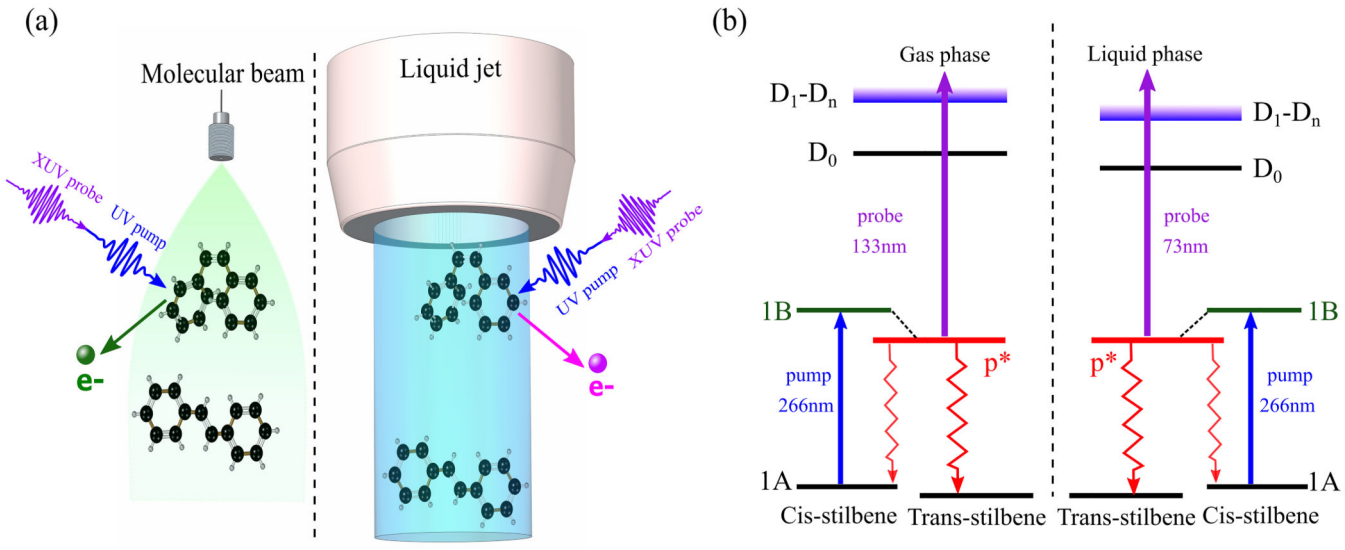

Figure 1. Schematic illustration of the experimental methods

Panel a) illustrates TRPES in the gas and liquid phases, highlighting their direct comparison. Panel b) shows a Jabłoński-type diagram illustrating the neutral and cationic electronic states that contribute to the TRPES during the *cis-trans* photoisomerisation of stilbene.

Europe PMC Funders Author Manuscripts

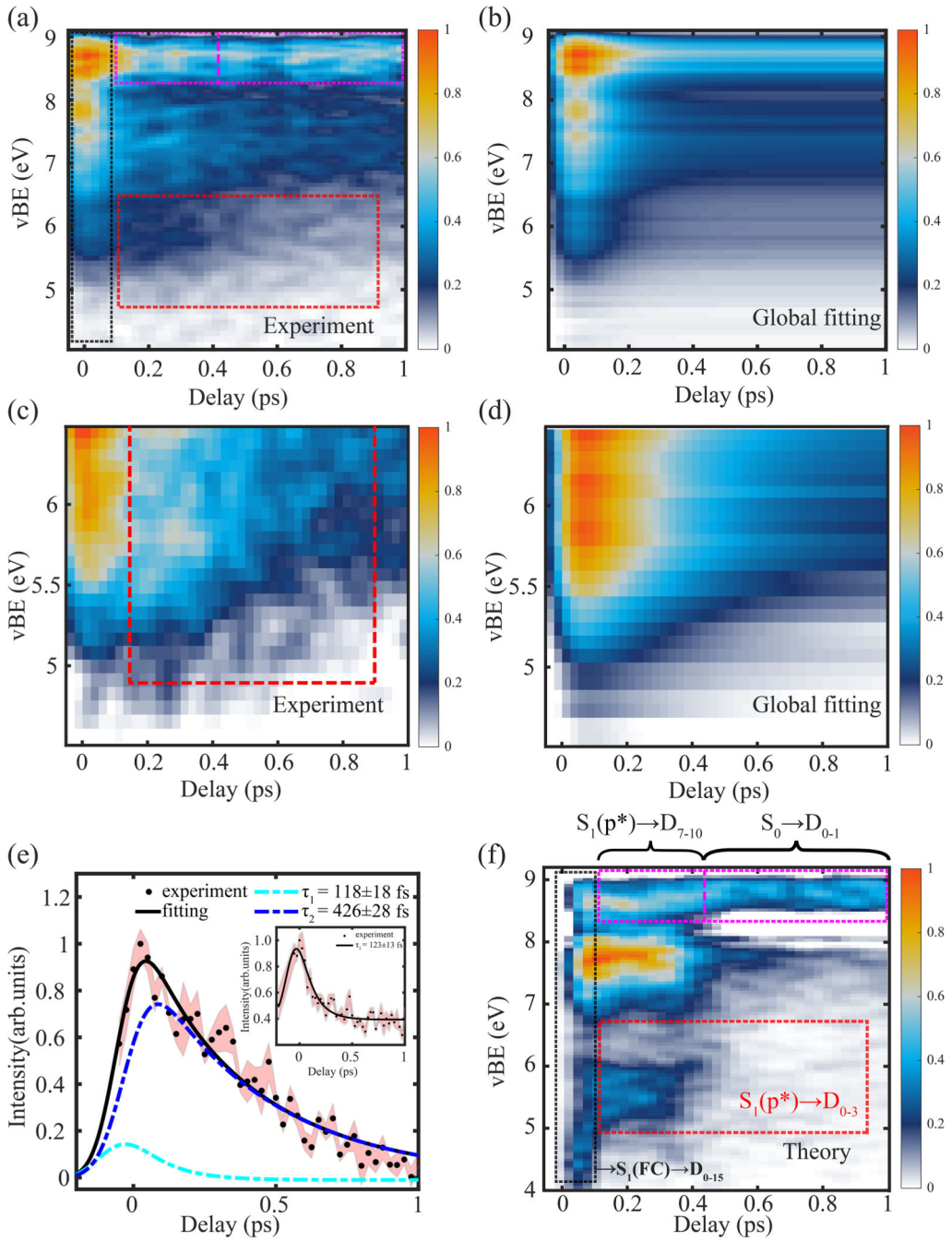

Figure 2. Time-resolved photoelectron spectra of the photoisomerisation of gaseous *cis*-stilbene.

Panel a) shows the measured spectrum with a noise threshold of 5% applied. The dashed boxes are the same as in panel f (theory), where their assignment in terms of initial and final states is given. A global fit of the data according to Eq.(1) is shown in panel b). The features between 8.5 – 9 eV, and 6.8 – 8 eV are very well described, but the signal between 5 – 6.5 eV decays too quickly. Therefore, this section was extracted and fitted separately. This high-energy part is shown in panel c), and the corresponding global fit according to Eq.(2) is shown in panel d). The one-dimensional decay profile of this fit is shown in panel e), the

inset of which shows the temporal profile of the global fit from panel b). The red-shaded area in (e) represents the error range (1 standard deviation) of the measured signal (black dots). Panel f) shows a histogram of the calculated ionisation energies weighted by Dyson norms along 200 trajectories of a non-adiabatic-dynamics simulation, including ionisation to 15 final states.

Europe PMC Funders Author Manuscripts

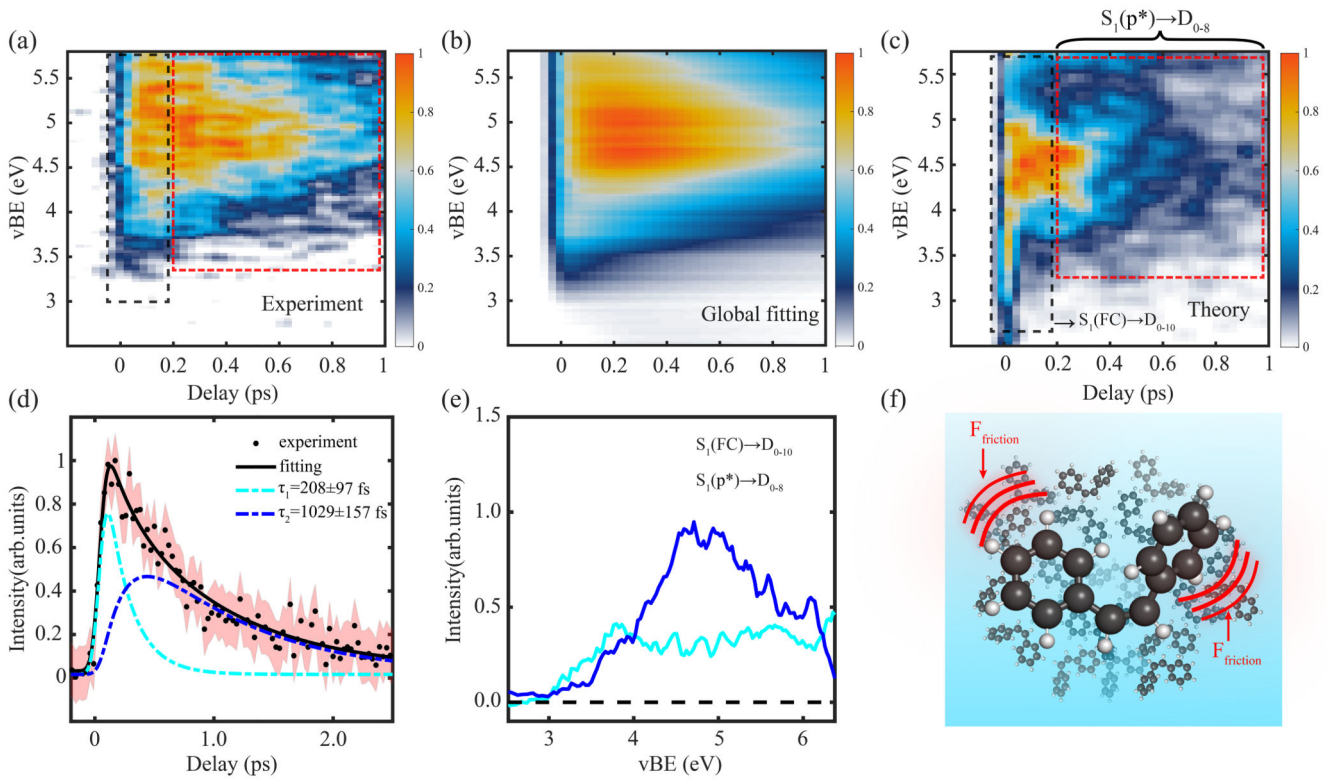

Figure 3. Time-resolved photoelectron spectra of the photoisomerisation of liquid *cis*-stilbene.
Panel a) shows the measured spectrum, with a noise threshold of 5% applied. The dashed boxes are the same as in panel f (theory), where their assignment in terms of initial and final states is given. A global fitting with a sequential biexponential model (Eq.(3)) is applied and shown in panel b). The one-dimensional decay profile of this fit is shown in panel d), with the decay-associated spectra shown in panel e). The red-shaded area in (d) represents the error range (1 standard deviation) of the measured signal (black dots). Panel c) shows a histogram of the calculated ionisation energies weighted by Dyson norms along 200 trajectories of a non-adiabatic-dynamics simulation, including ionisation to 15 cationic states. The calculations included frequency-independent friction, represented by a time constant $\tau = 0.5$ ps of the Langevin thermostat. The frictional effect is schematically illustrated in panel f).

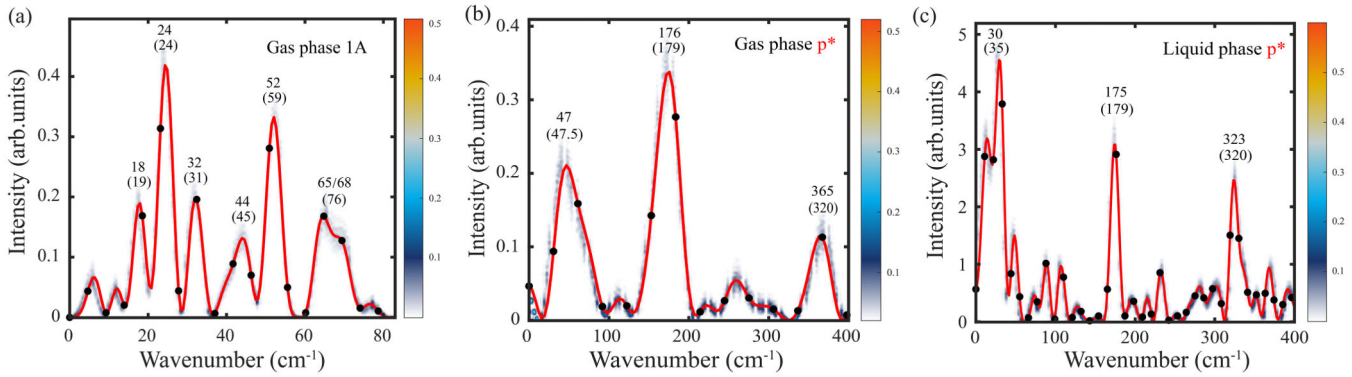

Figure 4. Fourier transform of the coherent oscillations observed in excited- and ground-state signals.

a) FFT of the ground-state oscillations shown in Supplementary Fig. 1, which is partially reproduced in Fig. 1a. b) and c) present the FFT spectrum obtained from the residuals of the p* region for the gas- and liquid-phase, respectively. The red lines represent the FFT of the experimental data that was zero-filled to improve the frequency resolution, whereas the black dots are the FFT of the non-zero-filled data. The density plots in blue quantify the sensitivity of the Fourier transform to white noise added in the time domain, as obtained from a Monte-Carlo simulation. The final relative error of the Fourier-transform amplitude in (c) amounts to 12%, as described in the SI, Section 1.2. The wavenumbers are compared to those obtained from other experiments (in parentheses, from Refs.[32, 33]). Additional details are given in the SM Section 1.2. and 7, where the FFT of the theoretical simulations is shown as Supplementary Fig. 12.

Europe PMC Funders Author Manuscripts

Europe PMC Funders Author Manuscripts

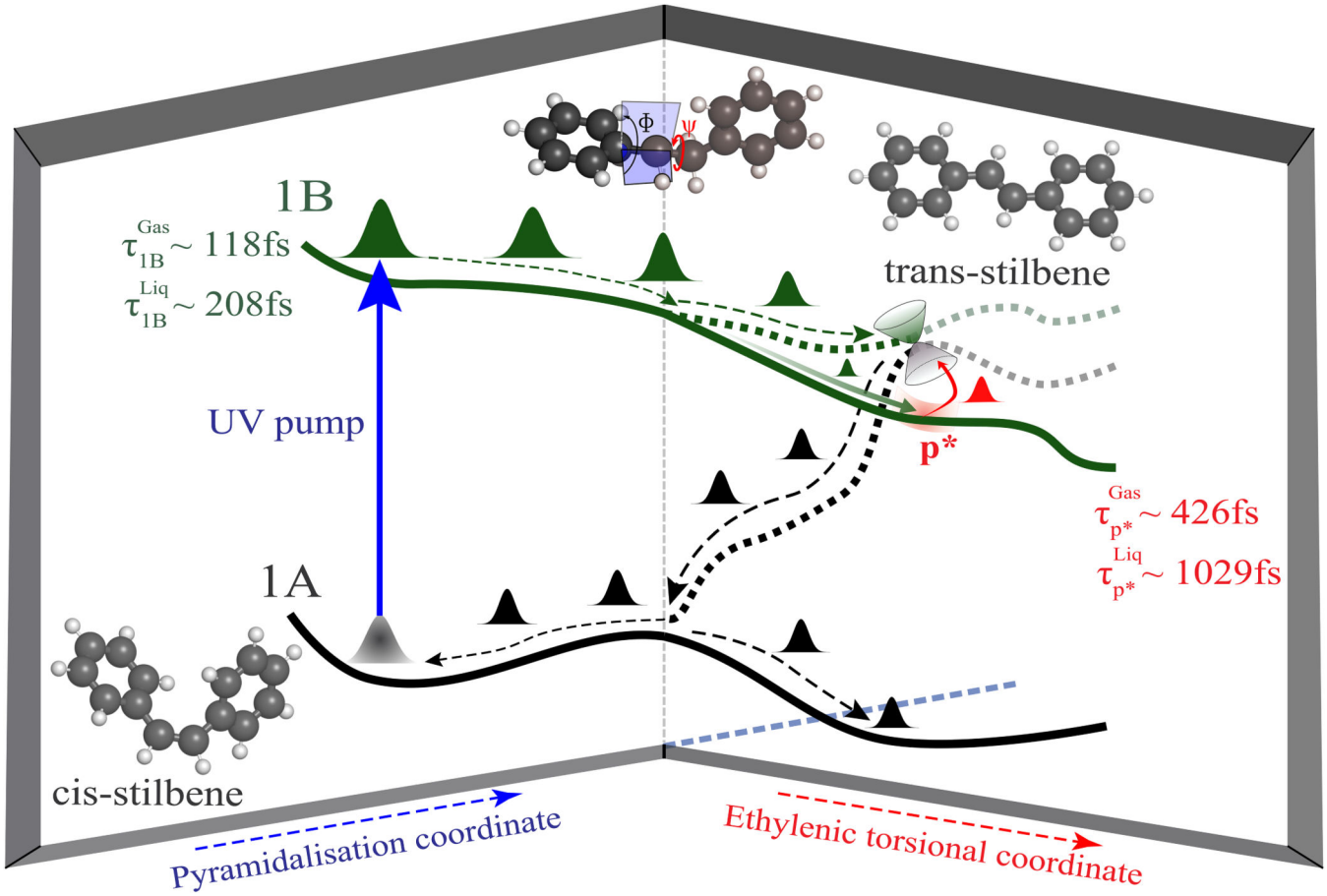

Figure 5. Summary of the excited-state dynamics of *cis*-stilbene.

Schematic representation of the potential-energy surfaces along the ethylenic pyramidalisation angle (Φ) and the dihedral angle of the ethylenic torsional motion (Ψ). The wave packet dynamics on the involved potential energy surfaces and across the most important conical intersections are shown, together with the time constants measured in the present work.